Research Square

Preprints are preliminary reports that have not undergone peer review.
They should not be considered conclusive, used to inform clinical practice,
or referenced by the media as validated information.

Tribocatalytic NiCrMo Superlattice Nanolayer Coatings for Wear Protection of Steel under Boundary Lubrication

Zaid A. Al Hassan
Northwestern University
Dieter Isheim
Northwestern University
D. Bruce Buchholz
Northwestern University
Tirzah Abbott
Northwestern University
Q. Jane Wang
Northwestern University
Yip-Wah Chung
ywchung@northwestern.edu

Northwestern University

Research Article

Keywords: Tribocatalytic coatings, Superlattice nanolayers, Boundary lubrication, Carbonaceous tribofilms, Wear resistance, 52100 steel

Posted Date: April 1st, 2026

DOI: https://doi.org/10.21203/rs.3.rs-9180491/v1

License: This work is licensed under a Creative Commons Attribution 4.0 International License.
Read Full License

Additional Declarations: No competing interests reported.

Abstract

Steel components operating under boundary lubrication often fail by wear, even when their bulk strength is adequate. Recent work has shown that high-chromium steels can exhibit unusually low friction and wear in hydrocarbon lubricants, not simply because of hardness, but because chromium promotes the formation of protective carbonaceous tribofilms during sliding. This observation suggests that tribochemical activity at the surface, rather than bulk alloy substitution, may provide a practical pathway to improved performance. Here, we report the design and evaluation of a nanocrystalline NiCrMo multilayer coating that combines chromium-driven tribocatalysis with mechanical robustness. Nichrome (Ni80Cr20) was selected to provide a chromium-rich, face-centered cubic matrix. To increase hardness and stabilize the nanostructure, molybdenum was introduced through both solid-solution alloying and an alternating nanolayer architecture consisting of NiCr(Mo) layers (~ 8 nm) separated by ultrathin Mo layers (~ 1 nm). This design suppresses columnar growth through repeated re-nucleation and limits grain size to less than 20 nm, yielding hardness values of 8.5–12.0 GPa. A graded interlayer was incorporated to improve adhesion to hardened 52100 steel substrates. Under boundary-lubricated reciprocating sliding (2 N, 2 Hz), the coating maintained a stable friction coefficient of 0.13–0.15 and reduced wear track width by approximately a factor of two relative to uncoated steel, corresponding to an estimated order-of-magnitude reduction in counterface wear. Raman analysis confirmed the formation of carbonaceous tribofilms. These results indicate that a mechanically stable, chromium-rich nanostructured coating can promote in situ formation of protective tribofilms and improve wear resistance without altering the bulk steel composition.

1 Introduction

Steel components operating under boundary-lubrication conditions are subject to wear-induced surface degradation. In this regime, the lubricant film thickness is less than the surface roughness, so much of the load is carried by asperity contacts. Under these conditions, surface damage accumulates unless some protective mechanism develops during sliding. One such mechanism is the formation of wear-protective tribofilms. As early as the 1950s, researchers at Bell Laboratories [1] observed the formation of amorphous brown deposits, then called “friction polymers”, during sliding of transition metals such as Cr, Mo, Pd, and Pt in organic vapors. These deposits formed as a result of the rubbing process itself, and the kinetics of formation were found to be strongly metal-dependent. More recently, Liao and co-workers [2] reported the formation of amorphous carbon-containing films when a CoCrMo alloy used in orthopedic implants was rubbed against itself in bovine serum. Similarly, Erdemir and co-workers [3] showed that when MoN-Cu or VN-Cu coated steels were slid in polyalphaolefin oil, carbonaceous tribofilms formed and led to lower friction and wear. Spikes and colleagues [4] further demonstrated that the thickness and performance of such films depend strongly on the steel composition.

In our recent work [5], we found that steels containing about 11 wt.% Cr, such as D2 tool steel, form carbon-containing tribopolymeric films during sliding in hydrocarbon lubricants. These films reduced wear by nearly an order of magnitude compared with 52100 steel of similar hardness. We attributed this

behavior to the presence of Cr_2O_3 on the surface under our test conditions. Cr_2O_3 is known to be catalytically active in hydrocarbon reactions. It is, in fact, the key component of the Phillips catalyst [6] used to polymerize ethylene to polyethylene, which accounts for roughly half of the world's polyethylene production. This observation suggested a simple idea: high chromium at the sliding surface may help catalyze the formation of a protective tribopolymeric film directly from the lubricant.

However, replacing an entire steel component with a high-chromium alloy is often impractical. Cost, manufacturability, heat treatment constraints, and qualification requirements can make wholesale substitution difficult. A more flexible approach is surface engineering, where the bulk material provides mechanical support, and the surface is tailored for specific functionality. This reasoning led us to explore a high-chromium coating that could (i) withstand contact stresses in mixed or boundary lubrication and (ii) maintain a chemically active surface to promote the formation of wear-protective tribofilms.

We selected nichrome (Ni80Cr20) as the starting composition. Its face-centered cubic structure offers better intrinsic toughness than many hard ceramic coatings, while its relatively high chromium content favors the formation of Cr_2O_3 during sliding. At the same time, several challenges must be addressed before such a coating can function effectively. First, nichrome is relatively soft. Its strength must be raised to at least match that of the 52100-steel substrate. Grain refinement to the nanocrystalline scale provides a clear strengthening route through the Hall–Petch effect; yet nanocrystalline materials are prone to grain growth, either during deposition (due to substrate heating) or during sliding (due to localized flash heating at asperity contacts). Microstructural stability is therefore a concern. Second, sputter-deposited coatings often develop a columnar microstructure because of limited adatom mobility [7]. Columnar boundaries can act as crack initiation sites and reduce mechanical integrity. Third, coatings with different crystal structure and coefficient of thermal expansion from the substrate may develop intrinsic stress. If this stress is too large, adhesion is compromised, and premature delamination can occur.

To address the first two challenges, we adopted a two-part strategy: alloying with Mo and introducing a superlattice nanolayer architecture. The addition of Mo provides solid-solution strengthening. The superlattice design consists of alternating nanolayers, several nanometers of NiCr followed by about one nanometer of Mo, repeated until the desired thickness is reached. This architecture forces repeated re-nucleation at each layer, interrupting columnar growth. Similar multilayer concepts [8, 9] have been used successfully in TiN/SiNx coatings to suppress columnar structures and increase rolling contact-fatigue lives. In our case, the repeated layering also limits the grain size to the same order as the individual layer thickness, thereby resulting in Hall–Petch strengthening.

Molecular dynamics simulations have shown that, given sufficient thermal energy, Mo atoms preferentially segregate to Ni grain boundaries [10]. Such segregation can thermodynamically stabilize nanocrystalline structures, as demonstrated in Ni-W [11, 12] and Cu-W [13] thin films. In our design, the superlattice architecture effectively places Mo at or near NiCr grain boundaries from the outset. In this

way, we reduce reliance on long-range diffusion, which is slow in Ni-based alloys [14], and promote grain-boundary stabilization by architectural design.

The third challenge, intrinsic stress and adhesion, is addressed through interfacial design. High interfacial energy increases the risk of delamination. As shown by Cahn and Hilliard [15], interfacial energy decreases as the interface becomes more diffuse. Instead of depositing the NiCrMo superlattice coating directly onto steel, we introduce a graded compositional transition between substrate and coating. This reduces the abruptness of the interface and lowers the interfacial energy.

Taken together, this NiCrMo superlattice coating represents a deliberate attempt to link chemistry and mechanics. Chromium provides the potential for tribochemical activity. Nanocrystalline refinement and Mo alloying provide strength. Superlattice architecture suppresses columnar growth and promotes stability. A graded interface improves adhesion. Rather than changing the bulk steel, we aim to create a surface that can both bear load and help generate its own protective film during sliding. In the following sections, we describe the coating architecture and experimental methods, and then present results in three areas: (1) suppression of columnar growth through the superlattice design; (2) nanostructural characterization, including phase composition, texture, grain size, and hardness; and (3) tribological performance during reciprocating sliding in a low-viscosity hydrocarbon fluid.

2 Materials and Methods

2.1 Materials and Sample Preparation

Two-inch magnetron sputtering targets of nichrome (99.9% purity), Cr (99.95% purity), and Mo (99.95% purity) were purchased from Kurt J. Lesker Company and used for all depositions. Coated substrates and uncoated counterface pins were fabricated from pre-polished AISI 52100-steel heat-treated to Rc 60 (Vickers hardness approximately 700, ~ 6.9 GPa). This steel was selected because it represents a widely used bearing material and provides a well-defined mechanical baseline for comparison. For selected structural and mechanical characterization experiments, particularly x-ray diffraction and nanoindentation, single-crystal silicon wafers were used as substrates. Their superior smoothness reduces surface roughness effects and minimizes variability unrelated to the coating itself. Prior to deposition, all substrates were ultrasonically cleaned in a 50:50 (v/v) hexane/acetone mixture for 15 minutes, rinsed with isopropyl alcohol, and this cycle was repeated three times. Immediately after the final rinse, substrates were then transferred to the sputtering chamber to minimize contamination.

2.2 Coating Architectures

Three coating architectures were examined to isolate the roles of alloying, multilayer design, and interfacial grading:

i. Monolithic NiCr-Mo: Ni80Cr20 containing 3.3 wt.% Mo, deposited as a single continuous layer.

ii. NiCr (+ 9 wt.% Mo)/Mo superlattice nanolayer coating, consisting of alternating nanolayers of *fcc* NiCr containing 9 wt.% Mo and *bcc* Mo. Typical layer thicknesses were 8.0 ± 1.6 nm for the NiCr layer and 1.0 ± 0.2 nm for Mo. This architecture was designed to suppress columnar growth and refine grain size through repeated re-nucleation.

iii. Superlattice nanolayer coating having the same architecture described above, deposited on 52100-steel substrate, with a 60-nm graded interlayer. The graded interlayer consisted of ~ 20 nm Cr, 20 nm NiCr, and 20 nm NiCr with Mo concentration graded linearly from 0 to 9 wt.% (Fig. 1). As noted in the Introduction, having a graded interlayer reduces the interfacial energy, thereby improving coating adhesion on the steel substrate.

Across the entire study, the total coating thickness ranged from ~ 0.5 to 2.2 μm, depending on the intended characterization:

- ~ 0.5–0.6 μm (on Si, no interlayer) for scanning electron microscopy, x-ray diffraction, and atom probe tomography
- ~ 1.2 μm (on Si, no interlayer) for nanoindentation
- ~ 1.2–2.2 μm (on 52100, with graded interlayer) for tribotesting

2.3 Coating Deposition

All coatings were deposited using a multi-target AJA magnetron sputtering system equipped with programmable shutters for all targets. The system base pressure ranged from the low 10^{-7} to high 10^{-8} Torr ($\sim 10^{-5}$ Pa). The Ar pressure during sputter-deposition was maintained at 3.5 mTorr (~0.5 Pa). Substrates were mounted on a rotating turntable (30 rpm) to promote thickness uniformity. A substrate bias of -100 V was applied to enhance adatom mobility and improve film density. Under these conditions, substrate temperatures were estimated to reach approximately 150–250°C during deposition. Monolithic coatings were produced by continuous co-sputtering of the NiCr and Mo targets to the desired thickness. Superlattice coatings were fabricated by alternating the opening and closing of shutters in front of NiCr and Mo targets, thereby generating the designed nanolayer sequence. Key deposition parameters are summarized in Table 1.

Table 1
Sputter deposition conditions

Parameter	Value
Deposition system	AJA magnetron sputter-deposition system
Working gas	Argon
Base pressure	Low 10^{-7} to high 10^{-8} Torr ($\sim 10^{-5}$ Pa)
Working pressure	3.5 mTorr ($\sim$0.5 Pa)
Substrate motion	Rotating turntable, 30 rpm
Substrate bias	-100 V
Substrate temperature during deposition	~ 150 to 250° C
Coating thickness range (study-wide)	0.5 to 2.2 μm

2.4 Thickness, Structural, Nanoindentation, and Adhesion Characterization

Coating thickness was measured by laser confocal microscopy using a masked step edge. The height difference between coated and uncoated regions was taken as the coating thickness. The same instrument was used to examine wear-track topography after tribotesting. The surface morphology and grain size of the coatings were characterized by field-emission scanning electron microscopy (FE-SEM), using a Hitachi SU8030 for silicon wafer samples and a Hitachi SU8700 for 52100 steel samples. Grain size distributions were determined using the line-intercept method.

X-ray diffraction (Cu Kα radiation, λ = 0.1541 nm) was used to determine the crystalline phase composition, preferred orientation, and multilayer periodicity. Data from high-angle θ-2θ scans in the Bragg-Brentano geometry were collected for phase and texture analysis. Selected scans at grazing incidence were performed to enhance the detection of Mo nanolayers and observe multiple reflections due to diffraction from superlattice layers.

Coating hardness was measured using a KLA nanoindenter equipped with a Berkovich diamond tip. The tip area function was calibrated using a fused quartz standard. Hardness values were extracted from the plateau regions of load-displacement curves using the Oliver-Pharr method [16], typically at indentation depths $\lesssim$ 10% of the coating thickness to minimize substrate influence. Unless otherwise noted, hardness values were obtained from coatings deposited on Si substrates to reduce roughness-induced scatter. Each reported value represents the average of three indents.

Adhesion was assessed qualitatively using Rockwell indentation by performing multiple indents onto the coated surface with a Rockwell C diamond indenter at 60 kgf. The region surrounding each indent was

examined for cracking, delamination, or spallation. The absence of such damage is taken as evidence of good adhesion.

2.5 Atom Probe Tomography

Specimens were prepared using focused-ion-beam (FIB) lift-out followed by annular milling standard techniques in a Thermofisher Helios 5 Hydra CX plasma-FIB/SEM to produce needle-shaped tips suitable for APT. Data were collected using a local electrode atom probe (CAMECA LEAP 5000 XS) in laser-pulsing mode (355 nm ultraviolet laser at 25 pJ laser pulse energy and 500 kHz repetition rate) under ultrahigh vacuum (2×10^{-7} Torr, 3×10^{-9} Pa) at cryogenic temperatures (40 K base temperature). Three-dimensional reconstructions were generated with the CAMECA IVAS3.8 software using standard reconstruction protocols, yielding three-dimensional maps of Ni, Cr, and Mo.

2.6 Tribological Testing and Analysis

Tribological performance was evaluated using a reciprocating tribotester (RTEC MFT-5000). The contact was fully immersed in F24 lubricant and tested under ambient laboratory conditions. An uncoated 5 mm radius 52100-steel pin was loaded against the coated flat at a normal load of 2 N. Sliding was conducted at 2 Hz with a 10 mm stroke length for 60 min. The corresponding maximum Hertzian contact stress was approximately 590 MPa. The coefficient of friction was recorded continuously throughout each test. After testing, the wear track was imaged by laser confocal microscopy.

Prior to examining the chemical nature of the carbon tribopolymeric films within and adjacent to the wear track by Raman spectroscopy, the tribotested substrates were rinsed with hexane to remove residual F24 lubricant and then allowed to air-dry at room temperature. Raman spectroscopy (HORIBA LabRAM HR) was performed with a 473-nm excitation laser and was calibrated to the Si standard at 520.7 cm^{-1} before each measurement session. Raw spectra were processed by cosmic-ray removal and a low-order polynomial baseline subtraction; no spectral smoothing was applied. A low laser power of 1.25 mW was used in all experiments to ensure that the observed data were not caused by laser-induced artifacts [17].

3 Results and Discussion

3.1 Elimination of Columnar Growth

Figure 2 shows a scanning electron micrograph of a 1.65-μm-thick monolithic NiCr coating containing 3.3 wt.% Mo deposited on Si. Pronounced columnar domains, approximately 150–300 nm in width, extend across the entire coating. Within each column, finer nanocrystalline grains (25–50 nm) are visible. While the nanocrystalline grain size is beneficial for strength, the larger columnar domains are undesirable. Boundaries between columns provide preferential paths for crack initiation and corrosion attack. As discussed earlier, columnar growth in sputtered metallic coatings arises primarily from limited adatom mobility during film growth [7]. Several conventional approaches can increase adatom mobility, including elevating substrate temperature, applying a more negative substrate bias to enhance ion

bombardment, or using energetic techniques such as HiPIMS (high-power impulse magnetron sputtering). However, each of these strategies introduces trade-offs. Higher temperatures can lead to grain coarsening. Increased ion bombardment may generate excessive compressive stress and promote delamination. HiPIMS can reduce deposition rate and introduce droplet formation.

Rather than modifying deposition energetics, we suppressed columnar growth through the superlattice architectural design. The superlattice nanolayer structure enforces repeated re-nucleation during growth. Deposition begins with several nanometers of *fcc* NiCr containing a few wt.% Mo, followed by an approximately 1 nm layer of *bcc* Mo. The crystallographic mismatch between *fcc* NiCr and *bcc* Mo interrupts structural continuity and forces re-nucleation. Before Mo columns can develop, deposition is switched back to NiCr. Repetition of this sequence produces a multilayer structure that prevents the persistence of columnar domains. Typical layer thicknesses were 8.0 ± 1.6 nm for NiCr and 1.0 ± 0.2 nm for Mo. Representative scanning electron micrographs (Fig. 3) obtained from a 500-nm-thick NiCr with 9 wt.% Mo/Mo superlattice nanolayer coating deposited on Si and 52100-steel substrate show a fully equiaxed nanocrystalline structure with no evidence of columnar domains. The multilayer architecture therefore achieves column suppression without relying on high-temperature or highly energetic deposition conditions.

3.2 Phase Composition and Texture

Figure 4 presents θ-2θ x-ray diffraction patterns from representative NiCr(Mo)/Mo superlattice coatings (600 nm thick) deposited on Si and 52100 steels. The dominant diffraction peak at 2θ = 43.84° corresponds to the NiCr (111) reflection. The (200) reflection near 51° is extremely weak. For a randomly textured *fcc* material, the expected intensity ratio I(200)/I(111) is approximately 0.5. The near absence of the (200) peak therefore indicates a strong (111) preferred orientation. This texture is consistent with minimization of surface energy during *fcc* film growth. The high-angle (222) reflection at 97.78°, visible in the pattern from the Si substrate, yields a lattice parameter of 0.3541 nm, in good agreement with reported values for NiCr alloys. Satellite peaks adjacent to the main (111) reflection, particularly clear for coatings deposited on Si, arise from the periodic multilayer structure. These features confirm the structural coherence of superlattice architecture. Weak reflections near 65° and 82° in the pattern from 52100 substrates originate from the steel.

In conventional Bragg-Brentano scans, the strongest Mo diffraction peak, corresponding to Mo (110), overlaps with the low-angle shoulder of the NiCr (111) peak. To resolve the Mo reflections more clearly, grazing-incidence x-ray diffraction (GIXRD) was performed (incidence angle = 0.5º). As shown in Fig. 5, the Mo (110) reflection at 2θ = 41.5° is clearly resolved, along with the Mo (200) reflection at 60.5°. These peaks correspond to an average Mo lattice parameter of 0.3067 nm, approximately 2.5% smaller than that of bulk Mo. Given the lattice parameters of NiCr and Mo, the Mo (110) planes likely adopt a Kurdjumov-Sachs orientation relationship with NiCr (111). In this configuration, the Mo nanolayer forms a strained epitaxial layer on the NiCr matrix. Based on bulk lattice constants, the resulting coherency strain in Mo is anisotropic, ranging from approximately − 2.6% along one in-plane direction to as much as

− 8.1% along another (assuming perfectly rigid NiCr matrix). The measured contraction of the Mo lattice parameter is consistent with this compressive coherency strain. We will return to this point later.

3.3 Grain Size and Layer Structure

The NiCr(Mo)/Mo superlattice nanolayer coatings consistently exhibit grain sizes below 20 nm. Grain-size distributions were determined from high-resolution SEM images (e.g., Fig. 3) using the line-intercept method. A representative distribution is shown in Fig. 6, yielding an average grain size of 17 ± 2 nm. This direct imaging approach provides a physically transparent measurement of in-plane grain dimensions and avoids assumptions inherent in diffraction line-broadening analysis (see Supplementary Information I).

Atom probe tomography (APT) provides complementary atomic-scale three-dimensional insight into both the multilayer architecture and the nanocrystalline structure. Figure 7(a) presents an APT reconstruction of a NiCr(Mo)/Mo coating deposited on 52100 steel, clearly revealing the periodic multilayer structure. The alternating NiCr(Mo) and Mo layers are readily distinguishable over multiple bilayer periods. A plan-view reconstruction of one NiCr(Mo) nanolayer is shown in Fig. 7(b). Grain boundaries are clearly visible. The contrast at these boundaries does not arise from elemental segregation; rather, it results from ion trajectory effects due to a variation of the local surface curvature at the grain edges at the time of field evaporation. The characteristic grain size observed in APT is 15–20 nm, consistent with the SEM line-intercept measurement. The agreement between these independent techniques confirms that the coatings possess a uniformly refined nanocrystalline structure.

Although APT can provide an estimate of layer spacing, quantitative determination requires assumptions about atomic density, typically taken from bulk values, which may not strictly apply to thin films. To avoid this uncertainty, the multilayer period was determined using low-angle x-ray diffraction. At sufficiently small angles of incidence, diffraction arises from the periodic stacking of nanolayers rather than from atomic lattice planes. The relationship between diffraction order *n* and angle θ is given by (see Supplementary Information II):

$$\sin^2\theta = \frac{n^2\lambda^2}{4L^2} + 2\delta$$

where θ = angle of incidence as measured from the surface, λ = 0.1541 nm (Cu Kα x-ray wavelength), *L* the multilayer period, and δ correction to the refractive index μ (= 1 − δ) for x-rays. Figure 8(a) shows the low-angle diffraction pattern obtained from a 1.15-μm-thick superlattice nanolayer coating on 52100 steel. The diffraction maxima occur at much smaller angles than those used for high-angle phase analysis. Plotting $\sin^2\theta$ versus n^2 as shown in Fig. 8(b) yields a linear relationship. The multilayer period extracted from the slope is 7.6 nm for this coating. This value is consistent with the designed bilayer structure (8.0 ± 1.6 nm for NiCr and 1.0 ± 0.2 nm for Mo, allowing for interfacial mixing and deposition variability). Taken together, SEM, APT, and low-angle x-ray diffraction provide mutually consistent evidence of well-defined nanocrystalline grain structure and multilayer periodicity.

3.4 Hardness

The mechanical response of the superlattice coatings was evaluated by nanoindentation. Figure 9 shows the measured hardness as a function of indentation depth from a representative 1.2-μm-thick NiCr(Mo)/Mo coating deposited on Si. A well-defined plateau is observed at approximately 9.4 GPa, indicating that substrate influence is negligible in this depth regime. Across multiple depositions, hardness values ranged from 8.5 to 12.0 GPa. The observed variation is likely associated with run-to-run differences in deposition rate and, consequently, small variations in individual layer thickness. Most important, these hardness values exceed that of the 52100 steel substrates and counterface pins used in tribological testing (≈ 7 GPa). The coatings therefore provide load-bearing capability comparable to, and in most cases greater than, the underlying steel. This ensures that tribological performance is not limited by insufficient mechanical support from the coating.

3.5 Coating Adhesion and Tribological Performance

In Section 3.2, we described the epitaxial relationship between NiCr(111) and Mo(110), which promotes strong bonding between adjacent nanolayers. At the same time, this coherency gives rise to lattice strains in the range of 2.6–8.1%. Strains of this magnitude can compromise adhesion to the steel substrate, particularly under the high shear stresses encountered during tribological testing. To mitigate this risk, we introduced a compositionally graded interlayer between the steel substrate and the NiCr(Mo)/Mo superlattice coating, as outlined in the Introduction. A graded interface reduces interfacial energy and distributes strain more gradually across the coating-substrate boundary. The coating architecture is shown in Fig. 1 and described in Section 2.2 (iii).

Figure 10 compares Rockwell indentation responses (60 kgf) for coatings deposited with and without the graded interlayer. The contrast is unambiguous. For the graded architecture, no cracking or delamination is observed either within or surrounding the indent. The indentation profile is smooth and continuous, indicating that the coating remains well bonded under severe localized deformation. In contrast, coatings deposited directly on 52100 steel without the graded interlayer exhibit extensive cracking and clear delamination around the indent perimeter. These results demonstrate that the graded multilayer design effectively preserves adhesion, even in the presence of substantial internal strain.

Representative friction traces obtained during fully immersed sliding in F24 hydrocarbon fluid further illustrate the functional benefit of the coating (Fig. 11). Uncoated 52100 steel exhibits a progressive increase in coefficient of friction within the first 10 minutes of sliding, rising from 0.13–0.14 to 0.20–0.25. This behavior is typical of boundary lubrication, where wear and debris generation gradually degrade the interface. In contrast, coated 52100 steel maintains a stable coefficient of friction between 0.13 and 0.15 throughout the 60-minute test. The absence of friction increase during this period indicates that the coating stabilizes the sliding interface under these conditions.

Raman spectroscopy performed on deposits adjacent to the wear track (Fig. 12) reveals features between 1350 and 2000 cm^{-1}, characteristic of carbonaceous tribopolymeric films. Peaks between 250

and 900 cm^{-1} are derived from various transition metal oxides. The presence of carbon-based deposits supports the tribocatalytic mechanism proposed in the Introduction, in which Cr_2O_3 formed during sliding promotes hydrocarbon transformation into a wear-protective tribopolymeric film.

It should be noted that tribopolymeric films formed under boundary lubrication are typically heterogeneous and patchy rather than continuous, with local thickness evolving dynamically during sliding. As such, a single, well-defined film thickness is not expected. While post-test cross-sectional analysis could provide an estimate of local film thickness, the protective effect observed here arises from a dynamic balance between film formation and removal, rather than from a static coating of fixed thickness. Direct in situ measurement of film growth kinetics remains an important topic for future investigation.

Wear behavior follows the same trend. Across multiple experiments conducted under identical conditions, the average wear-track width decreases from 350 ± 50 μm for uncoated 52100 to 170 ± 10 μm for coated steel. Figure 13 shows a representative comparison after one hour of sliding. The reduction in wear-track width is substantial and reproducible. Direct measurements of pin wear volume were not performed in the present study; however, geometric scaling provides a reasonable estimate of the magnitude of improvement. In the pin-on-disk configuration, the wear scar diameter on the pin closely matches the wear-track width on the flat, as previously established for this geometry [5]. For a spherical pin, wear volume scales with the fourth power of the scar diameter. Thus, the approximately two-fold reduction in wear-track width observed in Fig. 13 implies, by simple geometric scaling, an order-of-magnitude reduction in pin wear volume for sliding against the coated steel. This dramatic reduction provides strong evidence that the tribopolymeric film generated at the coated interface is not merely present, but tribologically effective.

The NiCr(Mo)/Mo multilayer coating functions by enabling a tribocatalytic process. During sliding, Cr_2O_3 forms dynamically and catalyzes the transformation of hydrocarbon molecules into carbonaceous oligomers, which then coalesce into a load-bearing tribopolymeric film. Wear is suppressed when the rate of tribofilm formation exceeds the rate of film removal. This process necessarily involves finite kinetics. Hydrocarbon adsorption, catalytic transformation, and structural reorganization all require time between reversals in reciprocating motion. In the present study, tests were conducted at 2 Hz, corresponding to approximately 250–500 ms available for tribofilm development at a given location within the stroke. With increasing reciprocating frequencies, the time available for tribofilm formation would decrease. It is therefore reasonable to expect the existence of a critical frequency beyond which tribofilm formation cannot keep pace with removal, leading to diminished protection. Similarly, applied load may influence the kinetics of tribofilm formation and removal. Exploring these kinetic limitations represents a logical next step in understanding and defining the operating window of this tribocatalytic system.

4 Conclusions

In this study, we designed and evaluated a NiCr(Mo)/Mo superlattice nanolayer coating intended to couple mechanical robustness with tribochemical activity. The goal was not simply to increase hardness, but to engineer a surface capable of promoting its own wear protection under boundary-lubrication conditions. The major conclusions of this work are:

1. Architectural control suppresses columnar growth. The alternating NiCr(Mo)/Mo nanolayer structure forces repeated re-nucleation during deposition, eliminating columnar domains observed in monolithic coatings. SEM and APT confirm a uniform equiaxed nanocrystalline structure with sub-20-nm grain size.
2. Mechanical properties exceed substrate requirements. Coatings must be hard enough to provide load support comparable to or better than the substrate. In this work, the NiCr(Mo)/Mo coatings exhibit hardness values between 8.5 and 12.0 GPa, exceeding that of the 52100-steel substrate, ensuring adequate load-bearing capability under the contact stresses used in tribological testing.
3. Graded interlayers are essential for adhesion. The introduction of a compositionally graded transition layer effectively prevents cracking and delamination under Rockwell indentation, despite internal coherency strains associated with the multilayer structure.
4. Tribocatalytic activity leads to substrate friction and wear reduction. Under boundary-lubricated reciprocating sliding, the coating maintains a stable coefficient of friction (0.13–0.15) and reduces wear-track width by approximately a factor of two relative to uncoated steel. Because counterface wear scales with the fourth power of scar diameter, this corresponds to nearly an order-of-magnitude reduction in pin wear. Raman spectroscopy confirms the formation of carbonaceous tribopolymeric films at the sliding interface.

Taken together, these results demonstrate that a chromium-rich, mechanically stable nanolayer coating can promote in situ formation of protective tribofilms without the need to alter the bulk steel composition. The performance improvement arises from the deliberate integration of crystallography, nanostructure, interfacial design, and surface chemistry within a single framework. More broadly, this work suggests that tribological performance in boundary lubrication can be enhanced not only by increasing hardness, but by engineering surfaces that actively participate in tribochemical processes. Understanding the kinetic limits of this tribocatalytic mechanism, particularly at higher sliding frequencies and variable loads, represents a promising direction for future investigations.

Declarations

Funding Declaration

This work was supported by the U.S. Army Small Business Innovation Research Program Office and the Army Research Office under Contract No. W911NF-24-C-0004.

Author Contribution

Conceptualization: Z.A.A.H., Q.J.W., Y.-W.C.; Methodology: Z.A.A.H., Q.J.W., Y.-W.C.; Investigation: Z.A.A.H., D.I., D.B.B., T.A.; Formal analysis: Z.A.A.H., D.I., Q.J.W., Y.-W.C.; Visualization: Z.A.A.H., D.I.,; Writing-original draft: Z.A.A.H.; Writing-review and editing: Z.A.A.H., D.I., D.B.B., T.A., Q.J.W., Y.-W.C.; Supervision: Q.J.W., Y.-W.C. All authors reviewed and approved the final manuscript.

Acknowledgements

This material is based upon work supported by the U.S. Army Small Business Innovation Research Program Office and the Army Research Office under Contract No. W911NF-24-C-0004. This work made use of the MatCI Facility; the SPID and EPIC facilities of Northwestern University's NUANCE Center; and the Northwestern University Jerome B. Cohen X-ray Diffraction Core Facility. These facilities are supported by Northwestern University, the International Institute for Nanotechnology (IIN), and the MRSEC program of the National Science Foundation (NSF DMR-2308691) at the Materials Research Center of Northwestern University; the X-ray Diffraction Core Facility is also supported by the Soft and Hybrid Nanotechnology Experimental (SHyNE) Resource (NSF ECCS-2025633). EPIC is identified as RRID: SCR_026361, and the Jerome B. Cohen X-ray Diffraction Core Facility as RRID: SCR_017866. Atom probe tomography was performed using the LEAP 5000XS tomograph at the Northwestern University Center for Atom-Probe Tomography (NUCAPT, RRID: SCR_017770), acquired and upgraded through equipment grants from NSF-MRI (DMR-0420532), DURIP-ONR (N00014-0400798, N00014-0610539, N00014-0910781, N00014-1712870, and N00014-2312593), and DURIP-ARO (W911NF2110052). NUCAPT is additionally supported by the MRSEC program (NSF DMR-2308691), the SHyNE Resource (NSF ECCS-2025633), and the Paula M. Trienens Institute for Sustainability and Energy at Northwestern University. The authors gratefully acknowledge Menglei Jiang of QuesTek Innovations and Bob Hilty of Xtalic for helpful discussions and technical insight related to this work. The authors also thank Dr. Sumit Kewalramani for helpful discussions.

Data Availability

The data supporting the findings of this study have been presented in the figures and/or given within the article. Additional information is available from the corresponding author upon reasonable request.

References

1. Hermance, H.W., Egan, T.F.: Organic deposits on precious metal contacts. Bell Syst. Tech. J. **37**, 739–776 (1958)
2. Liao, Y., Pourzal, R., Wimmer, M.A., Jacobs, J.J., Fischer, A., Marks, L.D.: Graphitic tribological layers in metal-on-metal hip replacements. Sci. (80-). **334**, 1687–1690 (2011)
3. Erdemir, A., Ramirez, G., Eryilmaz, O.L., Narayanan, B., Liao, Y., Kamath, G., Sankaranarayanan, S.K.R.S.: Carbon-based tribofilms from lubricating oils. Nature. **536**, 67–71 (2016)

4. Pagkalis, K., Spikes, H., Jelita Rydel, J., Ingram, M., Kadiric, A.: The influence of steel composition on the formation and effectiveness of antiwear films in tribological contacts. Tribol Lett. **69**, 75 (2021)
5. Khan, A.M., Ahmed, J., Liu, S., Martin, T., Berkebile, S., Chung, Y.W., Wang, Q.J.: Formation of wear-protective tribofilms on different steel surfaces during lubricated sliding. Tribol Lett. **71**, 63 (2023)
6. McDaniel, M.P.: Chap. 3 - A Review of the Phillips Supported Chromium Catalyst and Its Commercial Use for Ethylene Polymerization, pp. 123–606. Academic, Cambridge (2010)
7. Messier, R., Venugopal, V.C., Sunai, P.D.: Origin and evolution of sculptured thin films. J. Vac Sci. Technol. **A18**(4), 1538–1545 (2000)
8. Chen, Y.H., Polonsky, I.A., Chung, Y.W., Keer, L.M.: Tribological properties and rolling-contact-fatigue lives of TiN/SiNx multilayer coatings. Surf. Coat. Technol. **154**(2–3), 152–161 (2002)
9. Chen, Y.H., Guruz, M., Chung, Y.W., Keer, L.M.: Thermal stability of hard TiN/SiNx multilayer coatings with an equiaxed microstructure. Surf. Coat. Technol. **154**(2–3), 162–166 (2002)
10. Li, Q., Zhang, J., Tang, H., Zhang, H., Ye, H., Zheng, Y.: Influence of Mo segregation at grain boundaries on the high temperature creep behavior of Ni-Mo alloys: an atomic study. Materials. **14**, 6966 (2021)
11. Detor, A.J., Schuh, C.A.: Tailoring and patterning the grain size of nanocrystalline alloys. Acta Mater. **55**, 371–379 (2007)
12. Detor, A.J., Schuh, C.A.: Microstructural evolution during the heat treatment of nanocrystalline alloys. J. Mat. Res. **22**, 3233–3248 (2007)
13. Du, Y., Li, L., Pureza, J.M., Chung, Y.W., Pradeep, K.G., Sen, S., Schneider, J.: Thermal stability of nanocrystalline grains in Cu-W films. Surf. Coat. Technol. **357**, 662–668 (2019)
14. Heijwegen, C.P., Rieck, G.D.: Diffusion in the Mo-Ni, Mo-Fe and Mo-Co systems. Acta Metall. **22**, 1269–1281 (1974)
15. Cahn, J.W., Hilliard, J.H.: Free energy of a nonuniform system. I. Interfacial Free Energy. J. Chem. Phys. **28**, 258–267 (1958)
16. Oliver, W.C., Pharr, G.M.: An improved technique for determining hardness and elastic modulus using load and displacement sensing indentation experiments. J. Mat. Res. **7**, 1564–1583 (1992)
17. Li, Y.S., Jang, S., Khan, A.M., Martin, T.V., Ogrinc, A.L., Wang, Q.J., Martini, A., Chung, Y.W., Kim, S.H.: Possible origin of D- and G-band features in Raman spectra of tribofilms. Trib Lett. **71**, 57 (2023)

Figures

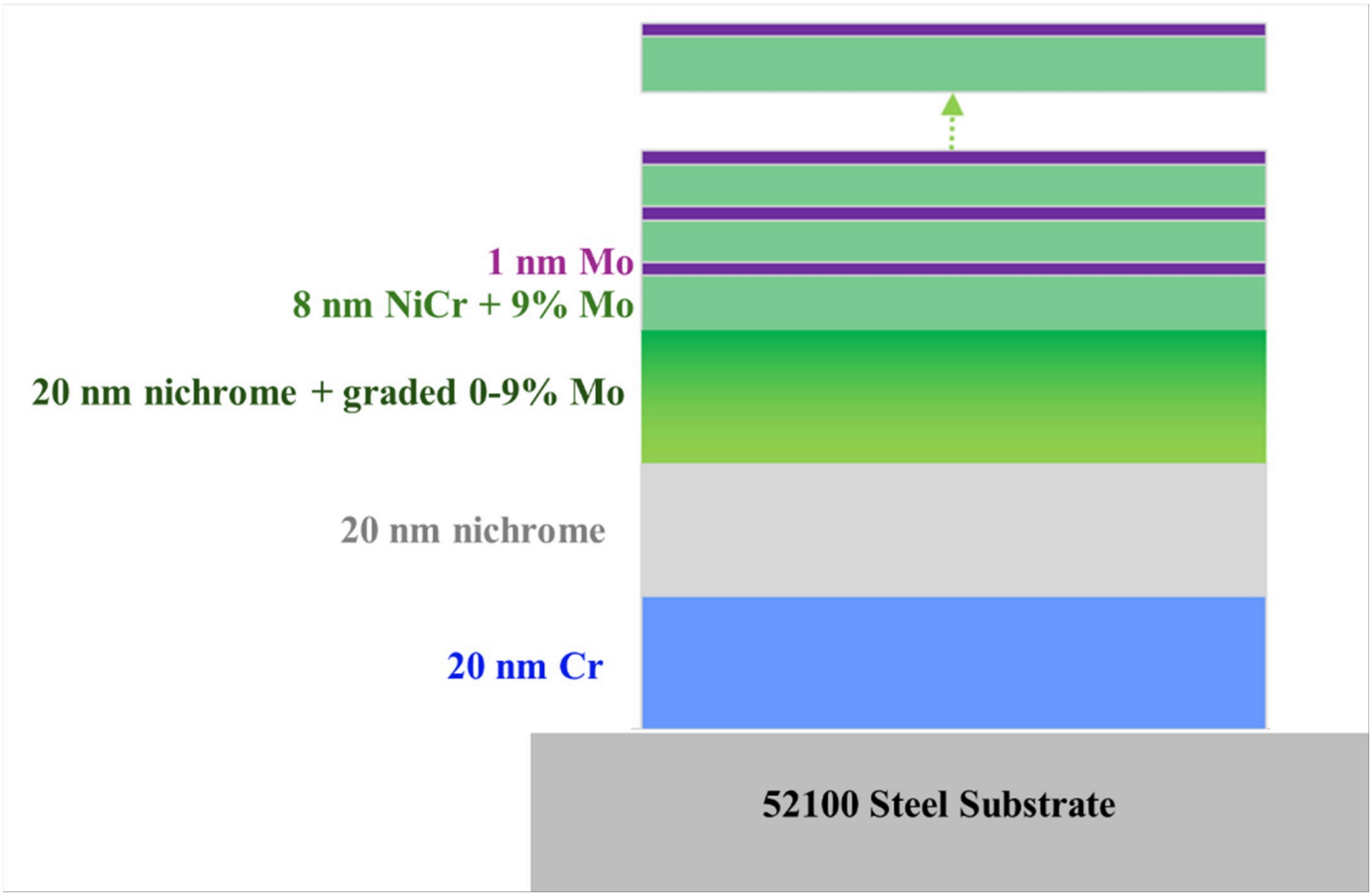


Figure 1

Coating architecture

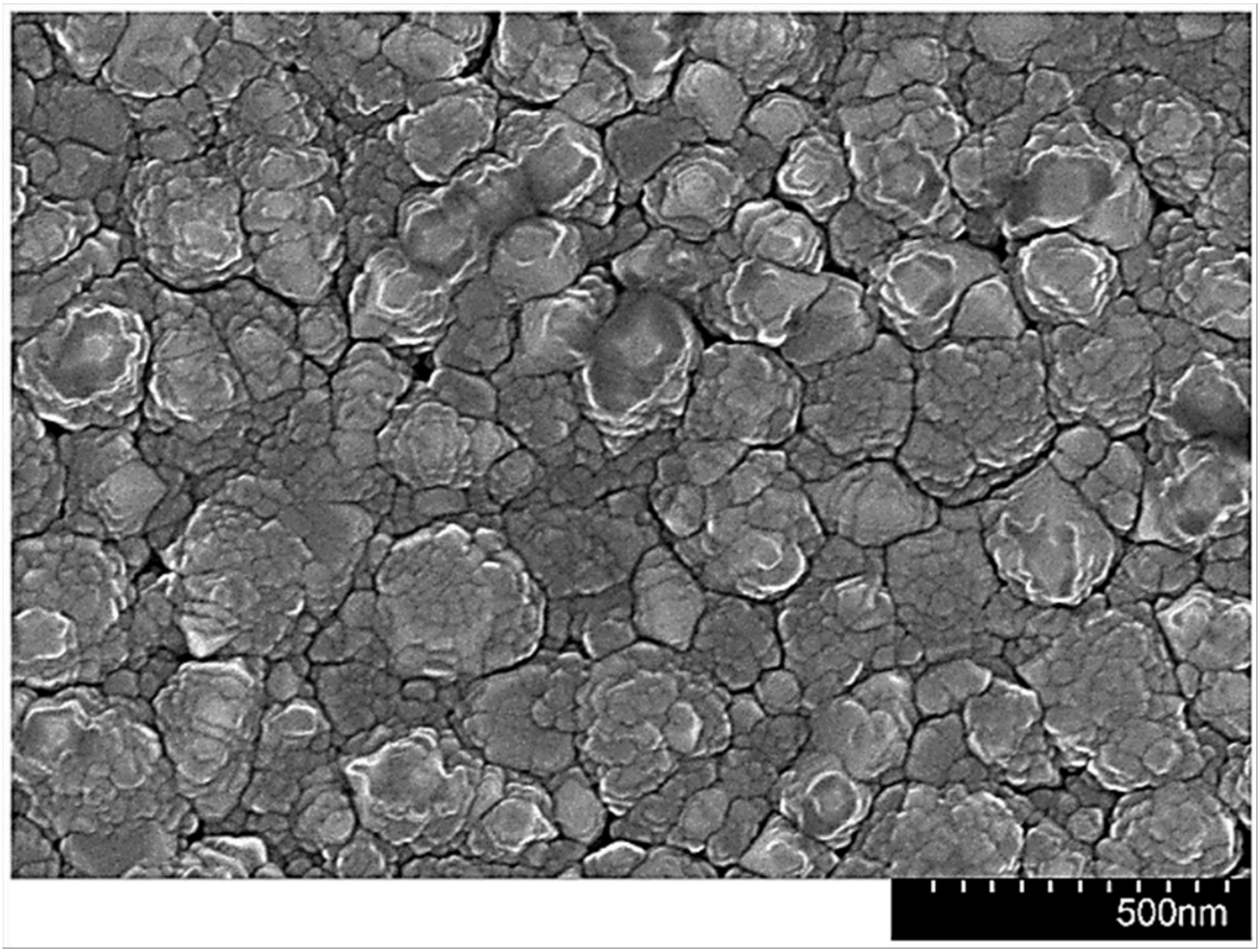


Figure 2

Scanning electron micrograph obtained from a 1.65-μm-thick NiCr coating with 3.3 wt.% Mo deposited on Si

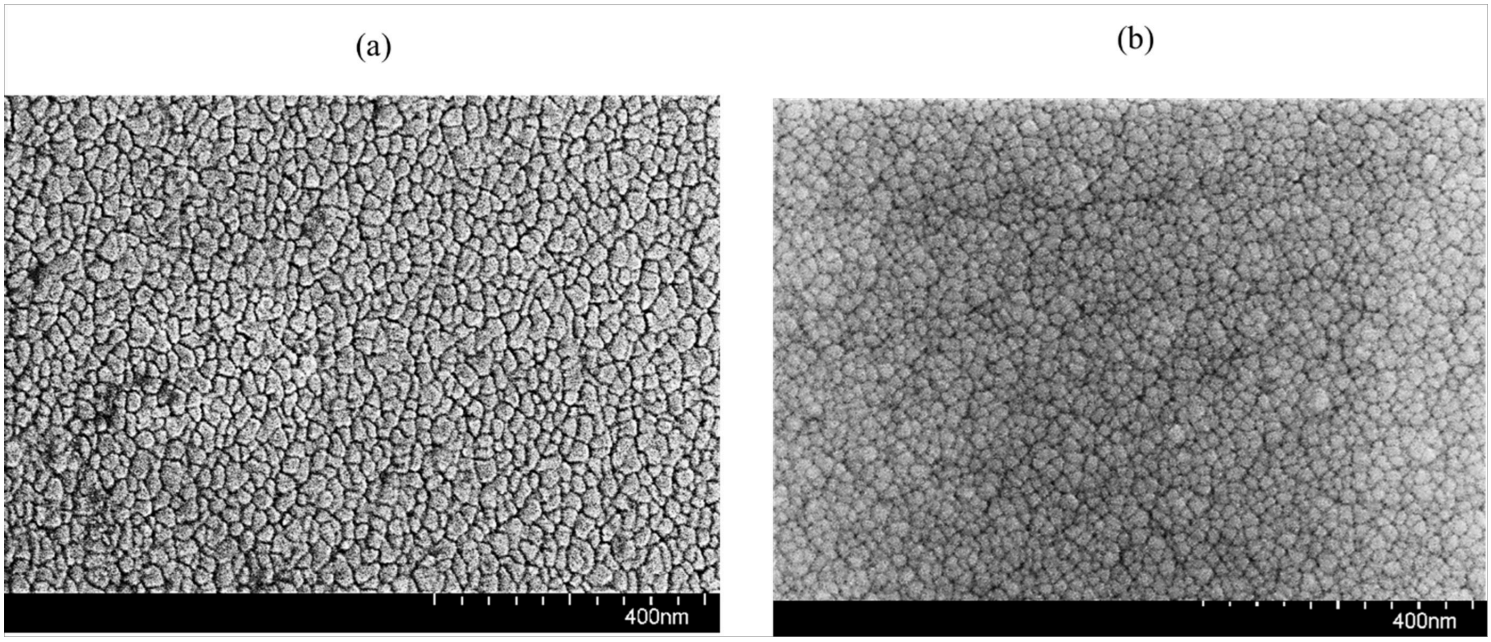


Figure 3

Plan-view SEM images of the surface morphology of a 500-nm-thick NiCr(Mo)/Mo superlattice nanolayer coating deposited on (a) Si and (b) AISI 52100 steel

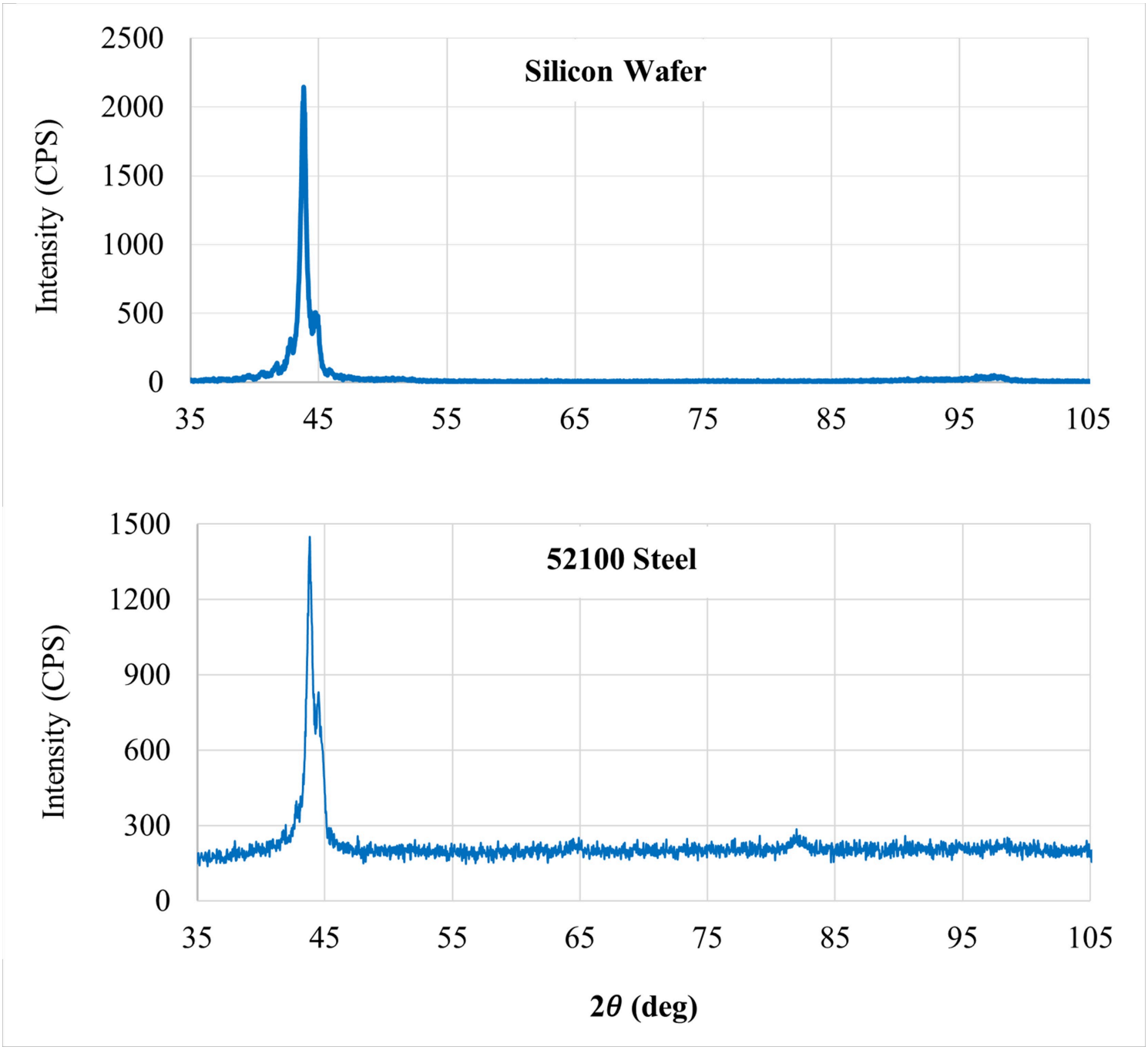


Figure 4

X-ray diffraction patterns obtained from a 600-nm-thick NiCr(Mo)/Mo superlattice nanolayer coating deposited on Si and 52100 substrates

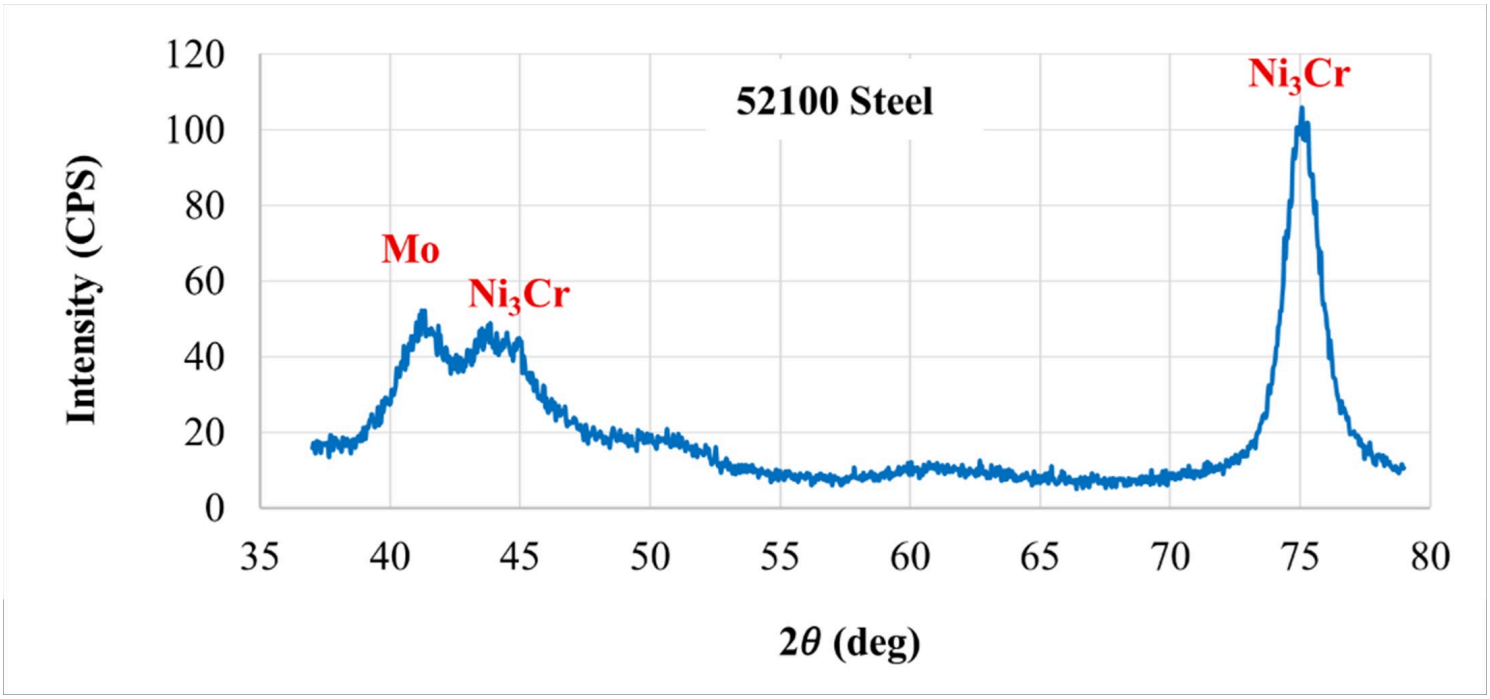


Figure 5

Grazing-incidence x-ray diffraction pattern obtained from the same NiCr(Mo)/Mo superlattice nanolayer coating deposited on 52100 steel as that shown in the lower panel of Figure 4

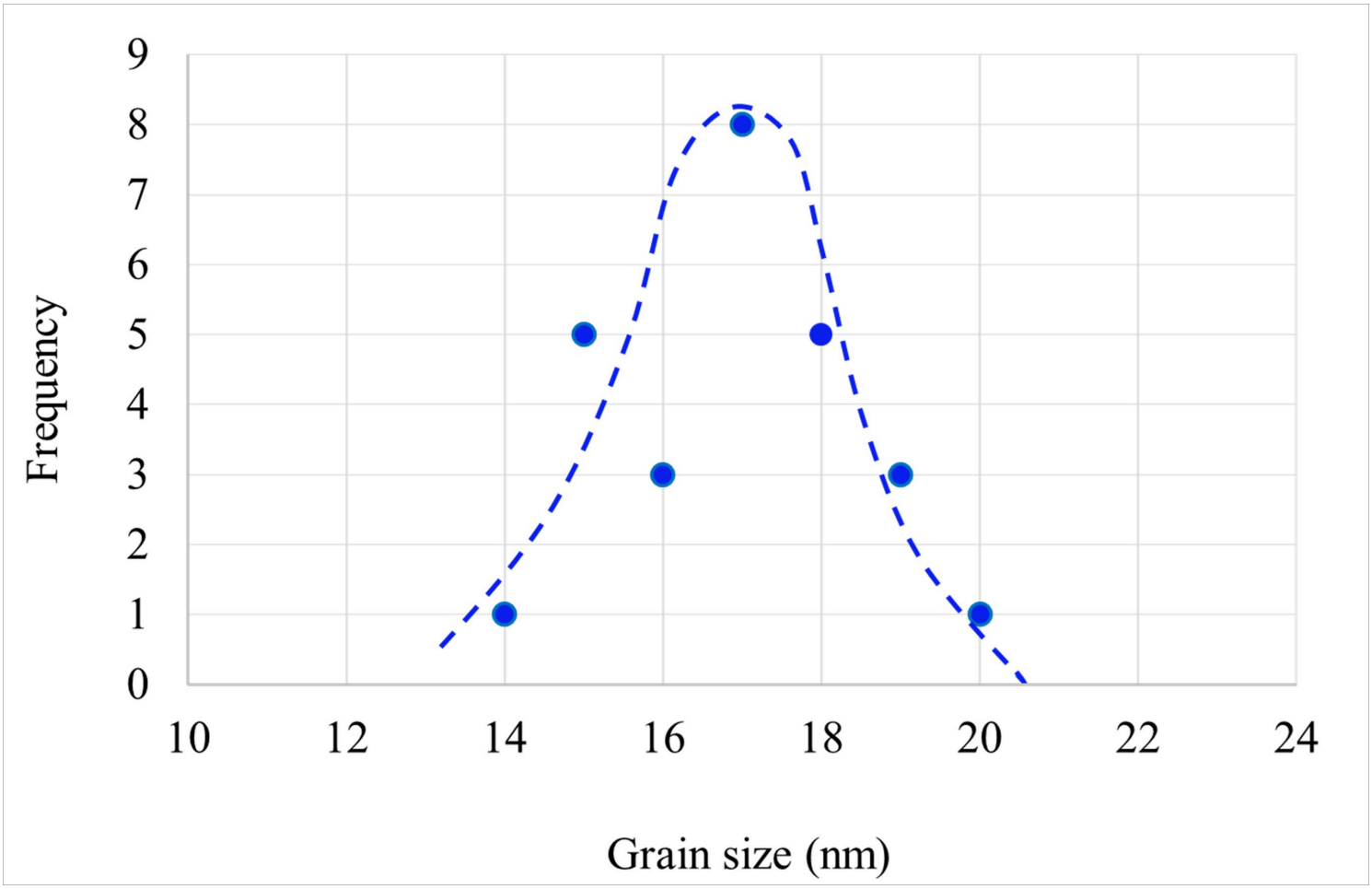


Figure 6

Grain size distribution for a representative 500-nm-thick NiCr(Mo)/Mo superlattice nanolayer coating deposited on Si

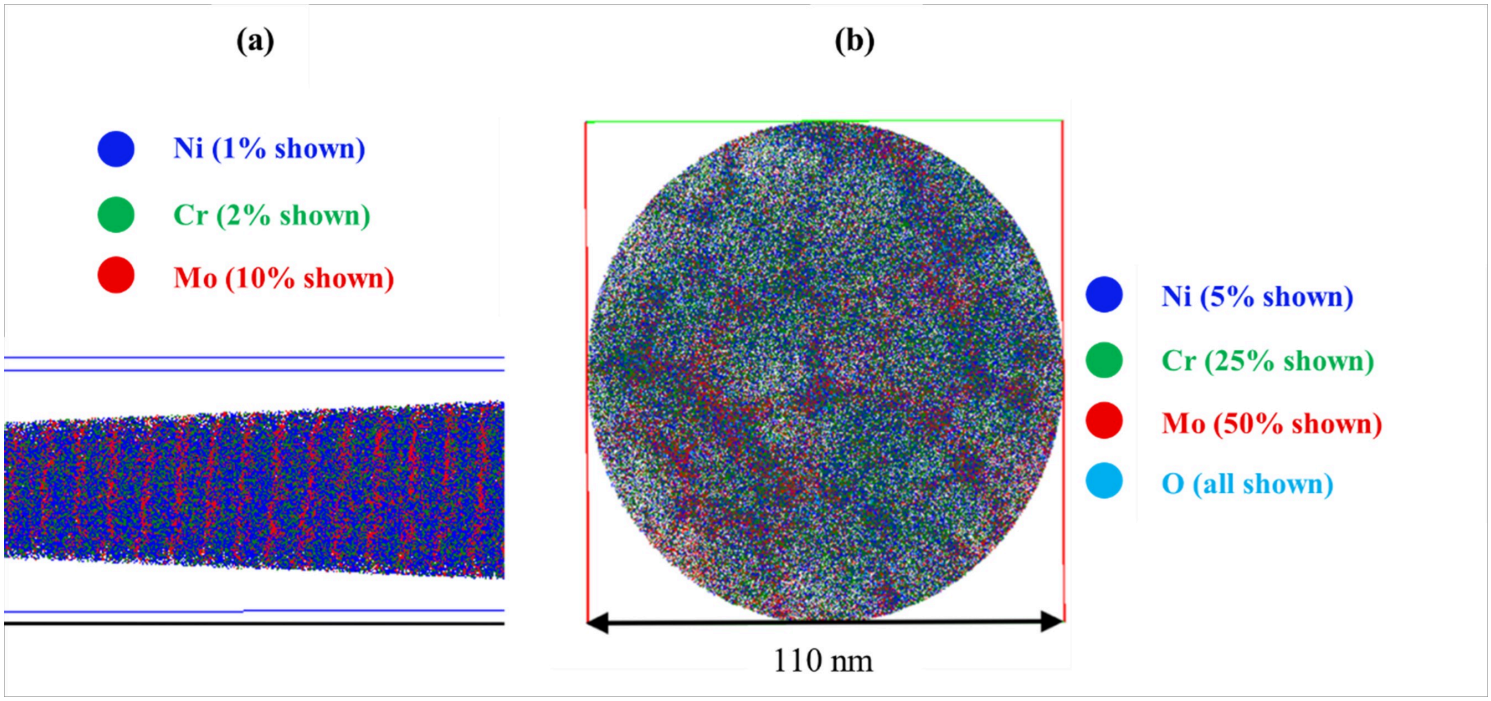


Figure 7

Atom probe tomography (APT) 3D atom-by-atom reconstruction images from a NiCr(Mo)/Mo superlattice nanolayer coating deposited on 52100 steel.

(a) Section of an APT reconstruction with the distribution of Ni, Cr, and Mo atoms in the NiCr(Mo)/Mo multilayer coating deposited on 52100 steel, revealing the periodic architecture.

(b) APT plan-view reconstruction of one of the NiCr(Mo) nanolayers, showing 15-20 nm grains due to grain-edge contrast

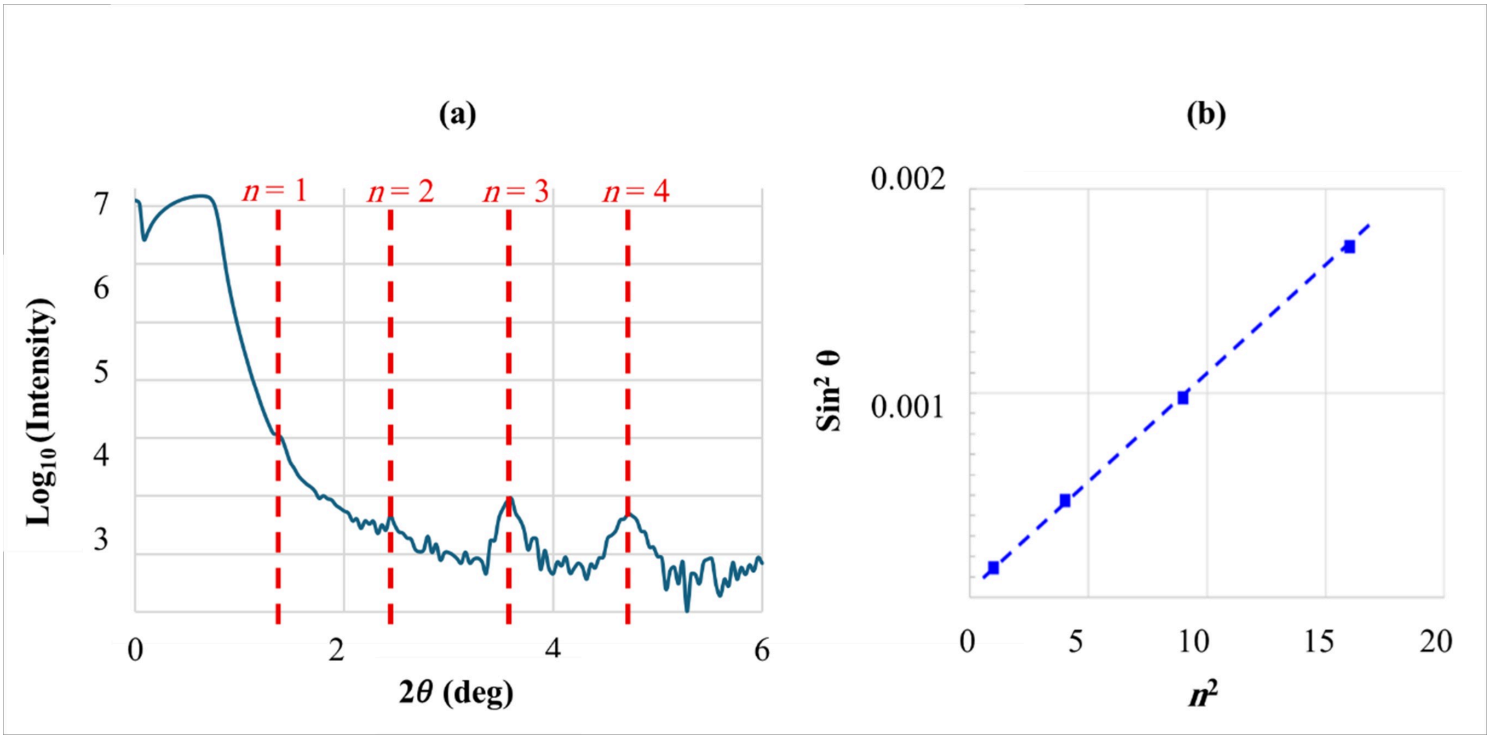


Figure 8

(a) Low-angle x-ray diffraction pattern obtained from a 1.15-micron-thick NiCr(Mo)/Mo superlattice nanolayer coating deposited on 52100 steel

(b) Plot of $\sin^2\theta$ versus n^2 based on data shown in Figure 8(a)

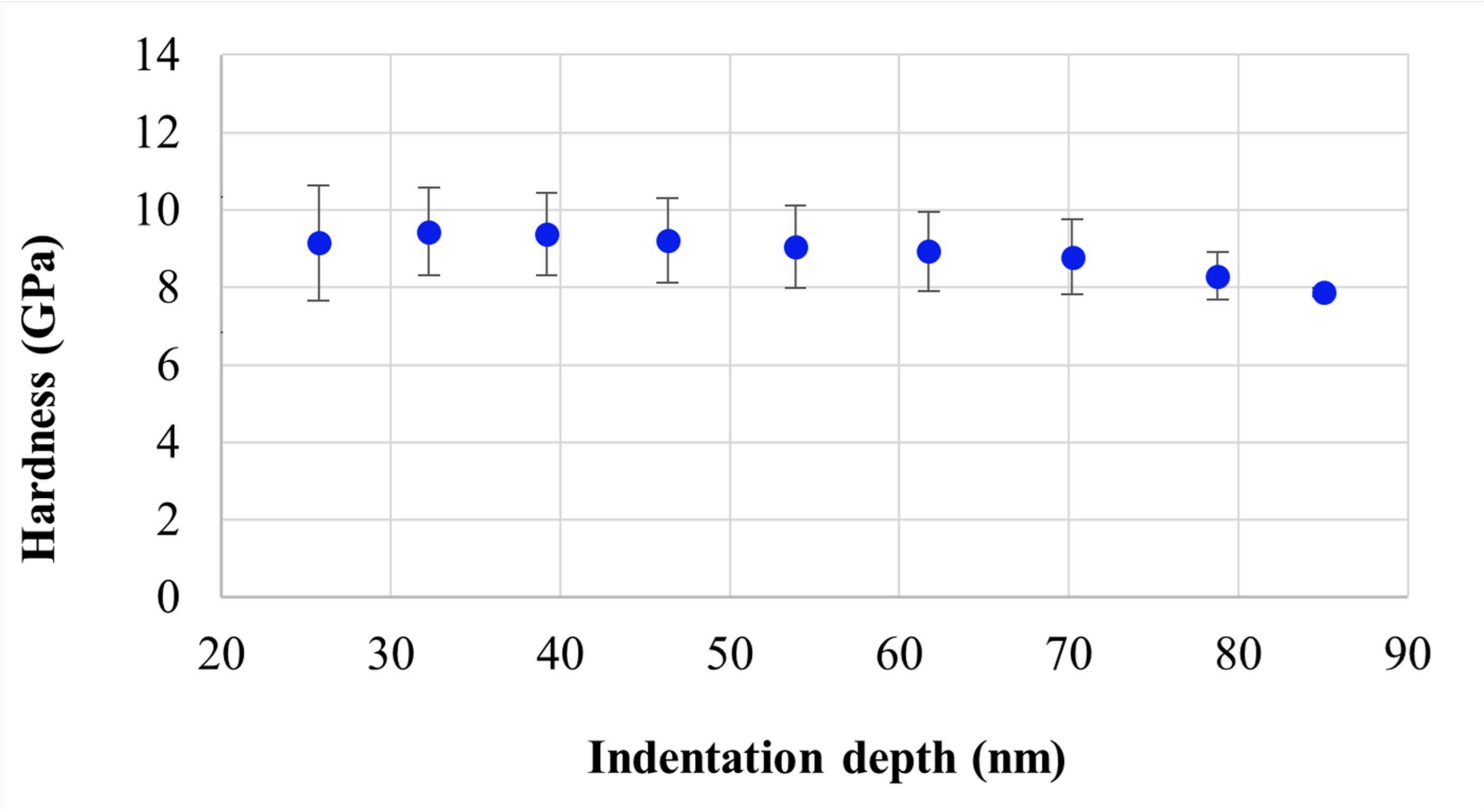


Figure 9

Nanoindentation hardness versus indentation depth for a 1.2-um-thick NiCr(Mo)/Mo superlattice nanolayer coating deposited on Si

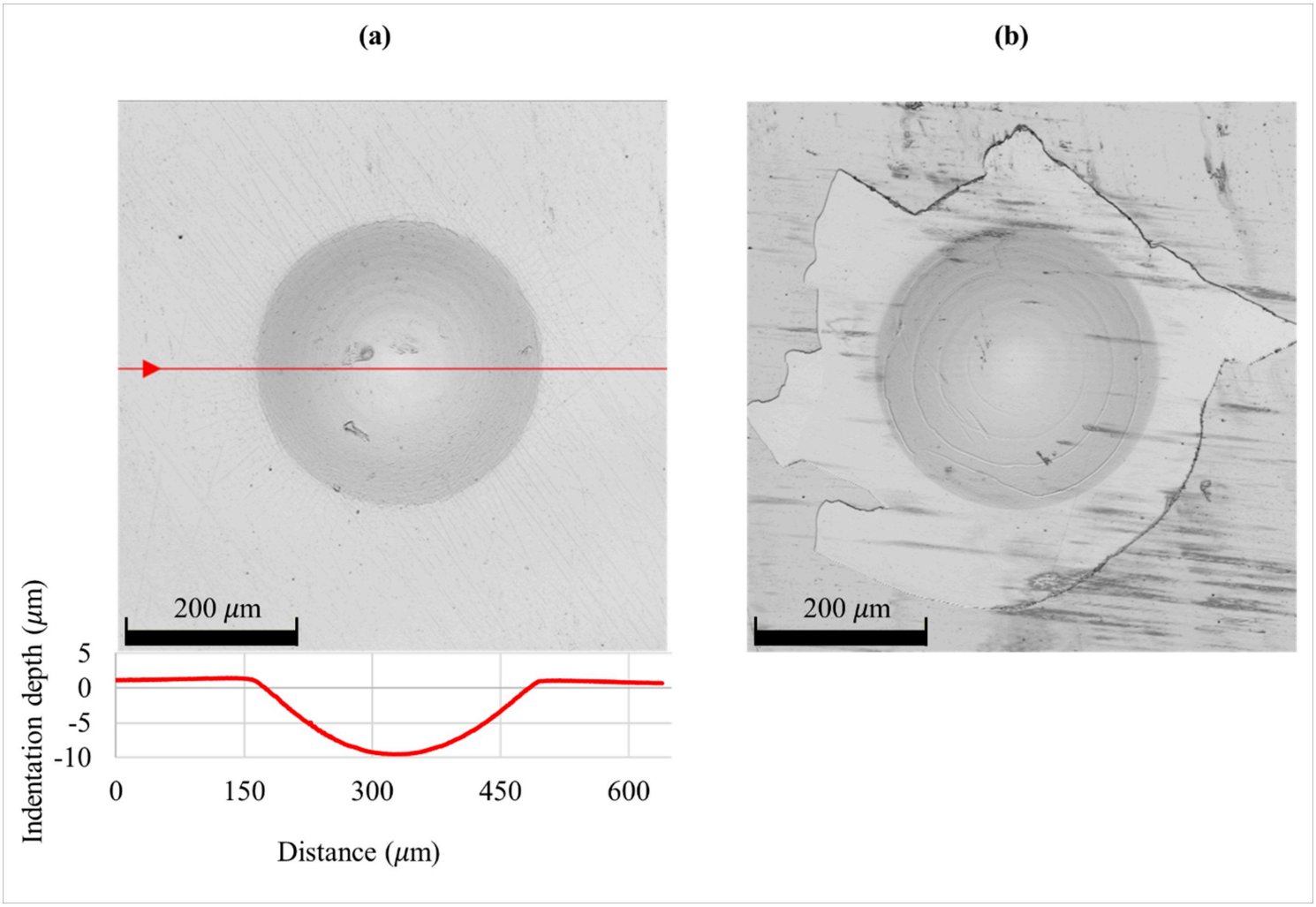


Figure 10

Optical micrograph of 52100-steel substrate coated with a 1.7-micron-thick NiCr(Mo)/Mo superlattice nanolayer coating (a) with the graded interlayer along with the bottom panel showing the corresponding topographical profile of the indent, and (b) without the graded interlayer. The indentation was produced using a Rockwell diamond indenter at 60 kg.

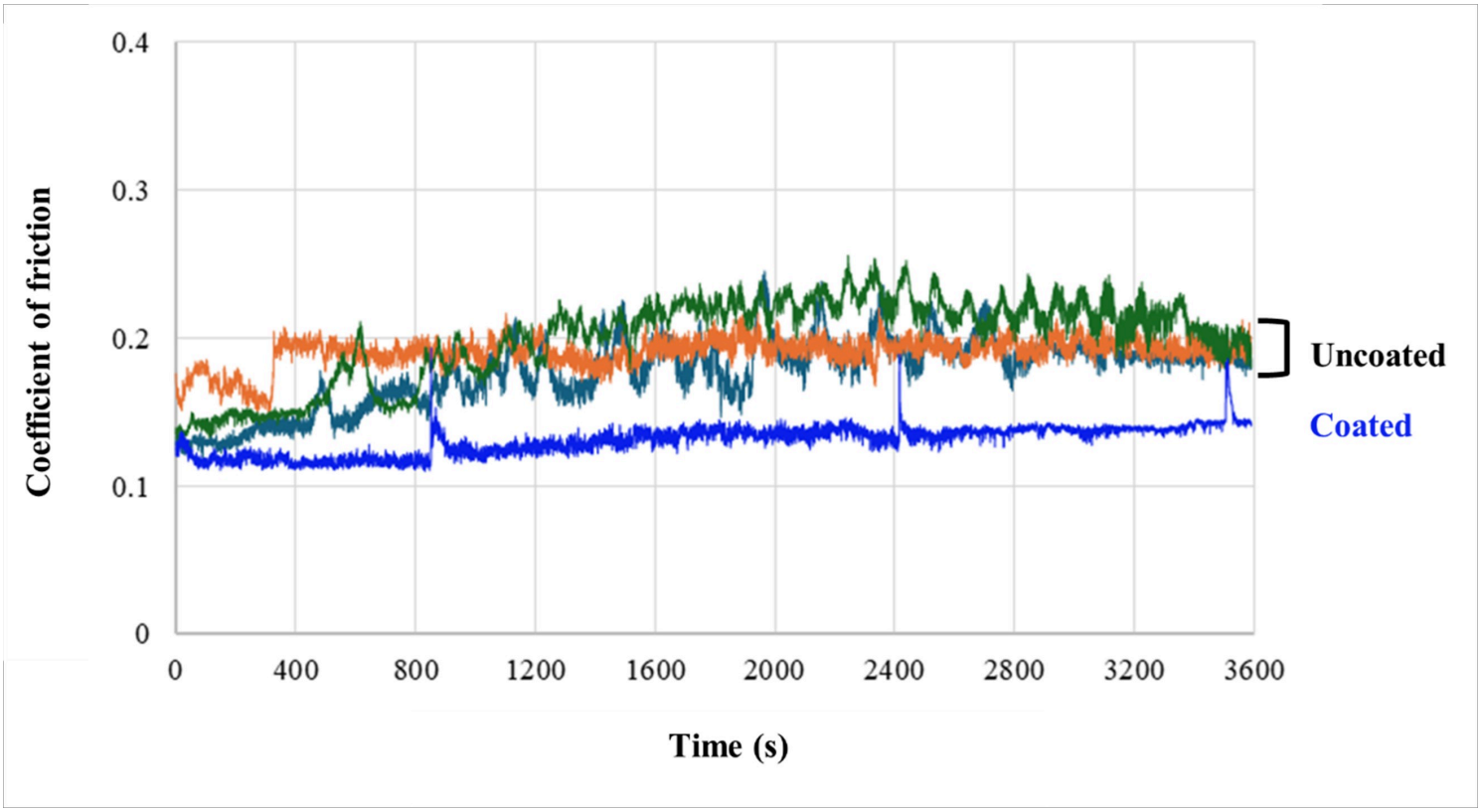


Figure 11

Coefficient of friction as a function of time for ball-on-flat sliding in F24 lubricant on uncoated 52100 steel and on the same steel coated with a 1.2-micron-thick NiCr(Mo)/Mo superlattice nanolayer coating (normal load 2N, reciprocating frequency = 2 Hz, stroke length = 10 mm, 52100 pin radius = 5 mm)

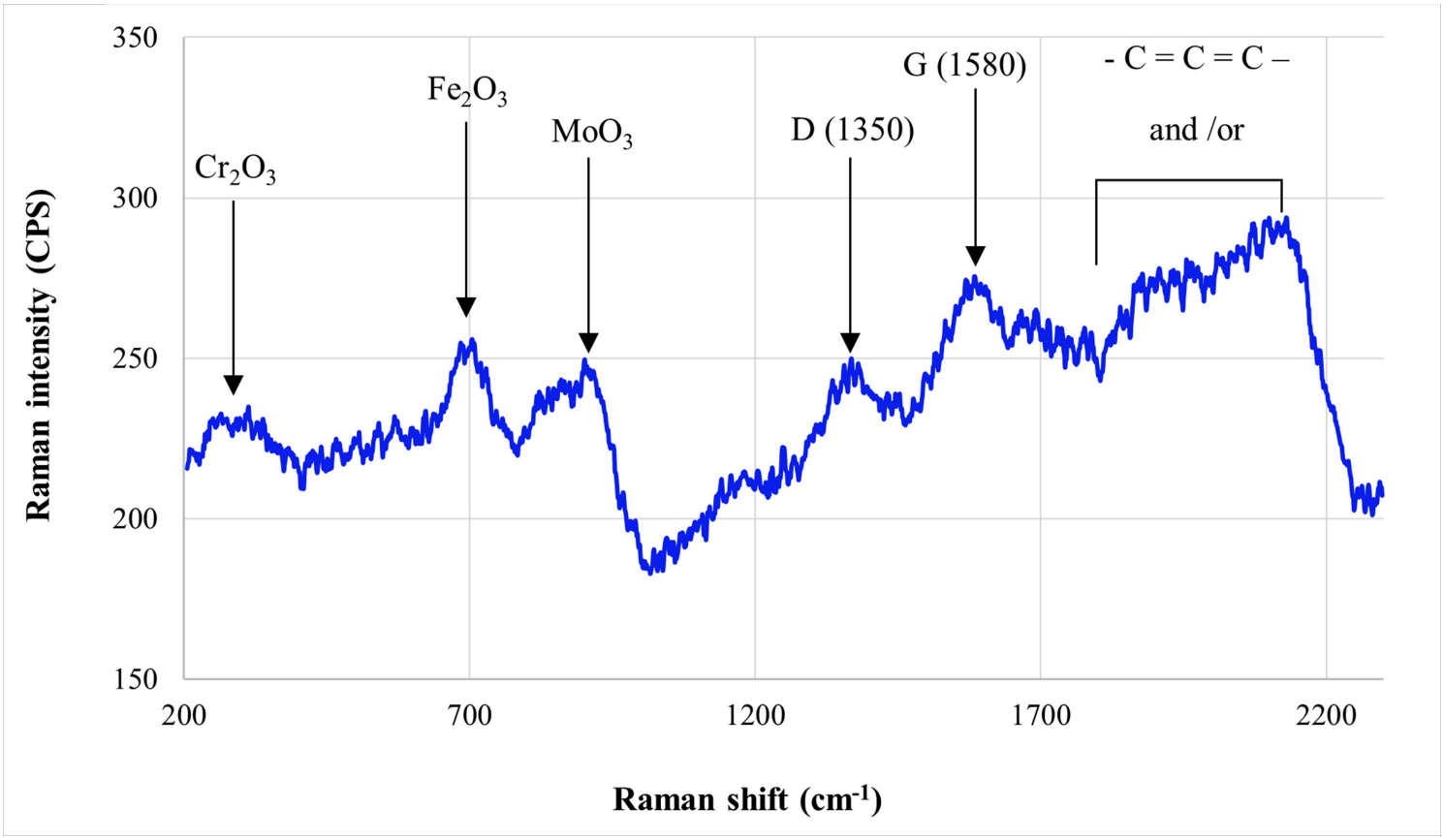


Figure 12

Raman spectrum obtained from deposits adjacent to the wear track on coated 52100 steel following the experiment shown in Figure 11. Spectral features from 250 to 900 cm^{-1} are due to various transition metal oxides, while features from 1350 to 2000 cm-1 are due to the carbon tribofilm

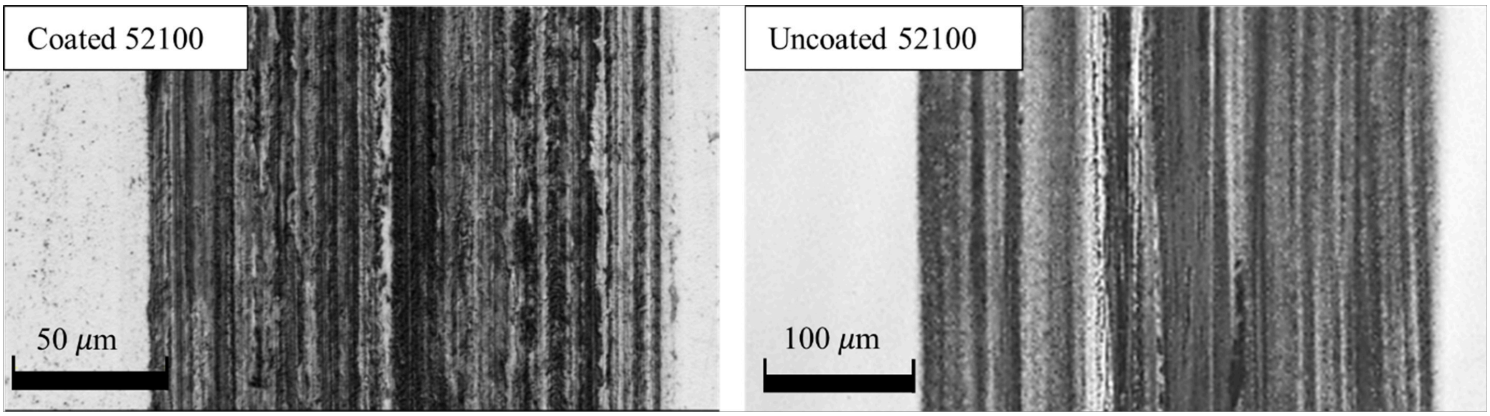


Figure 13

Optical micrographs of wear tracks obtained from coated and uncoated 52100 after one hour of tribotesting under the same conditions as listed in Figure 11. Note the difference in scale bars. For coated 52100, the wear track width is about 175 μm. For uncoated 52100, the wear track width is about 400 μm.

Supplementary Files

This is a list of supplementary files associated with this preprint. Click to download.

- NiCrMoTLSupplementarymaterial.docx